JACS
JOURNAL OF THE AMERICAN CHEMICAL SOCIETY
Article
Cite This: J. Am. Chem. Soc. 2017, 139, 15371-15376
pubs.acs.org/JACS

Cu_2IrO_3: A New Magnetically Frustrated Honeycomb Iridate

Mykola Abramchuk,[†] Cigdem Ozsoy-Keskinbora,[‡] Jason W. Krizan,[†] Kenneth R. Metz,[§] David C. Bell,[‡,⊥] and Fazel Tafti*[,†]

[†]Physics Department and [§]Chemistry Department, Boston College, Chestnut Hill, Massachusetts 02467, United States
[‡]Harvard John A. Paulson School of Engineering and Applied Sciences and [⊥]Center for Nanoscale Systems, Harvard University, Cambridge, Massachusetts 02138, United States

Supporting Information

ABSTRACT: We present the first copper iridium binary metal oxide with the chemical formula Cu_2IrO_3. The material is synthesized from the parent compound Na_2IrO_3 by a topotactic reaction where sodium is exchanged with copper under mild conditions. Cu_2IrO_3 has the same monoclinic space group ($C2/c$) as Na_2IrO_3 with a layered honeycomb structure. The parent compound Na_2IrO_3 is proposed to be relevant to the Kitaev spin liquid on the basis of having Ir^{4+} with an effective spin of 1/2 on a honeycomb lattice. Remarkably, whereas Na_2IrO_3 shows a long-range magnetic order at 15 K and fails to become a true spin liquid, Cu_2IrO_3 remains disordered until 2.7 K, at which point a short-range order develops. Rietveld analysis shows less distortions in the honeycomb structure of Cu_2IrO_3 with bond angles closer to 120° compared to Na_2IrO_3. Thus, the weak short-range magnetism combined with the nearly ideal honeycomb structure places Cu_2IrO_3 closer to a Kitaev spin liquid than its predecessors.

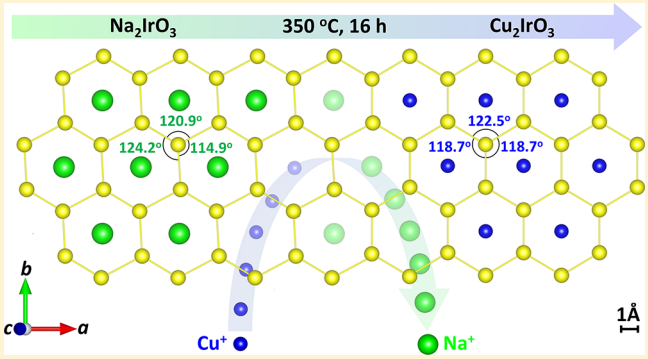

INTRODUCTION

The intricate relation between lattice structure and magnetism is a fascinating area of research in materials chemistry.[1] Geometric frustration is known to suppress magnetic ordering in triangular, pyrochlore, and Kagomé lattices.[1] The complete suppression of magnetic order in a $S = 1/2$ system gives rise to a quantum spin liquid.[2,3] In a seminal work, Kitaev proposed an intriguing theoretical model for quantum spin liquids by placing $S = 1/2$ Fermions onto a honeycomb geometry.[4] The *Kitaev model* is based on a bond-dependent ferromagnetic (FM) interaction $S_i^\gamma S_j^\gamma$, where i and j are neighboring sites at 120° and the bond dependence is imposed by $\gamma = x,y,z$. The special commutation relations between the Pauli matrices, $S^\gamma = \frac{\hbar}{2}\sigma^\gamma$, frustrate this interaction and give rise to a spin liquid. The Kitaev model received more appreciation after the discovery of honeycomb iridates Na_2IrO_3 and Li_2IrO_3.[5,6] Both of these materials contained Ir^{4+} in an octahedral crystal field with effective $S = 1/2$ placed onto a honeycomb lattice, satisfying the basic requirements of the Kitaev model. However, both compounds showed robust antiferromagnetic (AFM) order at 15 K, therefore failing to become true spin liquids.[6,7] The AFM order was explained as a result of two competing interactions on the honeycomb lattice:[5] $\mathcal{H}_{ij}^\gamma = -KS_i^\gamma S_j^\gamma + J\mathbf{S}_i\cdot\mathbf{S}_j$. The K term is the famous Kitaev FM interaction corresponding to the spin liquid. The J term is a conventional Heisenberg AFM interaction corresponding to the AFM order. The relative magnitude of the two terms tunes magnetism from a Kitaev limit (spin liquid) to a Heisenberg limit (AFM order). The long-range AFM order in Li_2IrO_3 and Na_2IrO_3 shows they are closer to the Heisenberg limit. Nearly a decade of research failed to produce another alkali honeycomb iridate due to the large ionic radii of K, Rb, and Cs. We now present a new honeycomb iridate made not with another alkali but with a transition metal. We first describe the chemistry pathway to make metastable Cu_2IrO_3 with copper in the 1+ state. We then reveal a near-ideal honeycomb structure and a lack of magnetic ordering down to 2.7 K, suggesting an unprecedented proximity to the Kitaev limit.

Structurally, A_2IrO_3 honeycomb iridates are derivatives of the ABO_2 delafossite system which has two polytypes: the bilayer hexagonal (2H) polytype known as the $CuFeO_2$ structure and the trilayer rhombohedral (3R) polytype known as the $AgFeO_2$ structure.[8] The structural parent of the honeycomb iridate, Na_2IrO_3, is the bilayer delafossite $CuFeO_2$ with space group $P6_3/mmc$. $CuFeO_2$ has layers of edge-sharing FeO_6 octahedra stacked along [00l] and linked with linear CuO_2 dumbbells.[9] Two structural modifications occur in transition from $CuFeO_2$ (space group $P6_3/mmc$) to Na_2IrO_3 (space group $C2/c$). First, within each layer, FeO_6 octahedra are replaced by $(Ir_{2/3}Na_{1/3})O_6$ octahedra. Every sodium atom is surrounded by

Received: July 3, 2017
Published: October 5, 2017

DOI: 10.1021/jacs.7b06911
J. Am. Chem. Soc. 2017, 139, 15371−15376

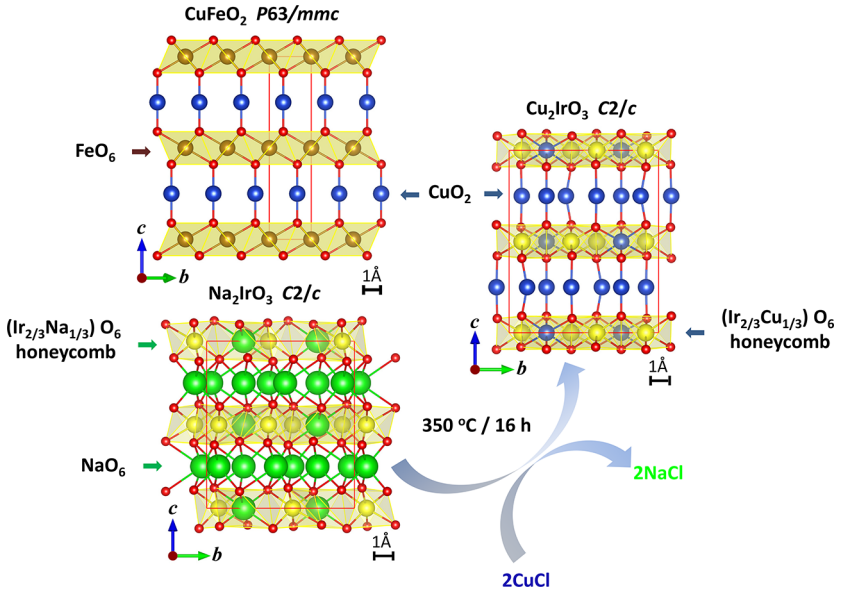

Figure 1. Structural and chemical relations between $CuFeO_2$, Na_2IrO_3, and Cu_2IrO_3. The structure of Cu_2IrO_3 consists of edge-sharing $(Ir_{2/3}Cu_{1/3})O_6$ octahedra in honeycomb layers, similar to Na_2IrO_3, and copper dumbbells between the layers, similar to $CuFeO_2$. The exchange reaction occurs according to eq 1 at moderate temperatures. Sodium atoms are replaced by copper atoms both between the layers and within the honeycomb layers.

six iridium atoms, whereas every iridium has three nearest neighbor iridium atoms. This arrangement gives rise to a planar honeycomb structure which accommodates two Ir for each Na. To emphasize the honeycomb ordering, the structural formula of Na_2IrO_3 can be written as $Na_3(NaIr_2)O_6$.[10] The second structural modification occurs between the layers where CuO_2 dumbbells in $CuFeO_2$ are replaced by distorted NaO_6 octahedra in Na_2IrO_3 (Figure 1).[11] Historically, the crystalline and the magnetic structures of Na_2IrO_3 have been tuned by either substituting the iridium with other transition metals[12] or by the isovalent substitution of Na^+ with Li^+.[13,14] We succeeded to fully substitute Na^+ by Cu^+ through a topotactic reaction between Na_2IrO_3 and CuCl to make the new honeycomb iridate Cu_2IrO_3 (Figure 1). Structural refinement shows that Cu_2IrO_3 crystallizes in the $C2/c$ space group with honeycomb layers of edge-sharing $(Ir_{2/3}Cu_{1/3})O_6$ octahedra similar to Na_2IrO_3, but these layers are linked by the CuO_2 dumbbells as in $CuFeO_2$ (Figure 1). The formation of CuO_2 dumbbells is due to the eclipsed stacking of adjacent layers which aligns oxygen atoms in a linear coordination with the interlayer copper atoms. As a result, Cu_2IrO_3 acquires a hybrid structure between Na_2IrO_3 and $CuFeO_2$. Chemical analyses indicate the absence of sodium in the structure, confirming a complete exchange of sodium with copper, even from within the honeycomb layer.

EXPERIMENTAL SECTION

Synthesis. The new copper iridate Cu_2IrO_3 was obtained through a metathesis reaction between sodium iridate (Na_2IrO_3) and copper(I) chloride (CuCl, Alfa Aesar, 99.999%). To synthesize Na_2IrO_3, a well-ground homogeneous mixture of sodium carbonate (Na_2CO_3, Alfa Aesar, 99.5%, dried at 120 °C for 24 h) and iridium oxide (IrO_2, Alfa Aesar, 99%) was prepared with the mole ratio of 1.15:1 and total mass of 300 mg. The mixture was placed in a covered alumina crucible and transferred to a muffle furnace. Preparation of the reaction mixture was carried out inside an argon-filled glovebox with O_2 and H_2O content <0.1 ppm. The crucible was heated at 3 °C/min to 800 °C, annealed at 800 °C for 48 h, then cooled at 10 °C/min to 600 °C, and quenched into the antechamber of the glovebox to avoid decomposition.[11] The resulting sample contained 1−2% of IrO_2 impurity and was purified by successive cycles of adding 5−10 mol % of Na_2CO_3, grinding, and annealing at 825 °C for 24 h. The ion exchange was performed by mixing Na_2IrO_3 and CuCl in the mole ratio 1:3 or 1:2.05 with no difference in the final product. The mixture with total mass of 150−300 mg was pelletized, placed in a covered alumina crucible, and sealed under vacuum in a quartz tube. The tube was slowly heated at 1 °C/min to 350 °C, kept at that temperature for 16 h, then cooled to room temperature at the same rate. In order to remove the excess of CuCl and NaCl, samples were subsequently ground into fine powders and washed five times with ammonium hydroxide (NH_4OH, Alfa Aesar, 28%) and twice with deionized water. After being washed, all samples were dried at room temperature under vacuum for 1 h. Cu_2IrO_3 was found to be stable in air with no changes of color or X-ray diffraction pattern after 3 weeks at ambient conditions.

X-ray Diffraction. Powder X-ray diffraction (PXRD) was performed using a Bruker D8 ECO instrument in the Bragg−Brentano geometry with a copper X-ray source (Cu Kα), a nickel filter to absorb the Kβ radiation, and with two 2.5° Soller slits after the source and before the LYNXEYE XE 1D energy-dispersive detector. Rietveld refinement on the PXRD pattern was performed using the FullProf suite.[15] Peak shapes were modeled with the Thompson−Cox−Hastings pseudo-Voigt profile convoluted with axial divergence asymmetry.

Electron Microscopy, Optical Spectroscopy, and Thermogravimetric Analysis. Energy-dispersive X-ray spectroscopy (EDXS) was performed using an EDAX detector installed on a JEOL JSM 6340F field emission scanning electron microscope (FESEM). Inductively coupled plasma optical emission spectroscopy (ICP-OES) was performed using the Agilent model 5100 VDV spectrometer operating in axial mode. For quantitative analysis with ICP-OES, sodium and copper standards with five different concentrations were made from NaCl and $CuSO_4{\cdot}5H_2O$ dissolved in deionized water. The experimental uncertainties were calculated by a propagation of error analysis using a linear direct calibration plot.[16] Thermogravimetric analysis (TGA) was performed using a NETZSCH analyzer (model STA 449 F1 Jupiter) to determine the oxygen content of Cu_2IrO_3. The sample was heated to 500 °C at 1 °C/min under a 20 mL/min flow of 5% H_2/Ar gas mixture to provide a reducing environment.

Physical Property Measurements. Magnetization in powder specimens was measured as a function of field and temperature by zero

DOI: 10.1021/jacs.7b06911
J. Am. Chem. Soc. 2017, 139, 15371−15376

field cooling and field cooling in a 7 T Quantum Design MPMS3. A low background brass holder was used to mount the powder material, and the measurements were performed in the DC mode. Four-probe resistivity measurements and heat capacity measurements on pressed pellets of Cu_2IrO_3 were performed in a Quantum Design Dynacool system.

RESULTS AND DISCUSSION

Chemical Composition. The synthetic goal was to completely replace Na^+ with Cu^+ in sodium iridate according to

$$Na_2IrO_3 + 2CuCl \rightarrow Cu_2IrO_3 + 2NaCl \quad (1)$$

In the first trial, we used 50% excess of CuCl and set the temperature to 400 °C to ensure a complete exchange. Later experiments revealed that lower temperatures (350 °C) and less excess CuCl (5%) worked equally well. The low temperature and the short duration of the exchange reaction prevented structural collapse, while copper atoms replaced sodium atoms. We tried solid-state synthesis from CuO and IrO_2 at high temperatures (700−900 °C) without success, which confirmed that topotactic reaction under mild conditions is the preferred method for making copper iridate (Figure 1). EDXS analysis on multiple samples confirmed the ratio Cu/Ir = 2:1. The sodium peak at 1.041 keV was absent in the EDXS spectrum (Supporting Information). To confirm the absence of sodium from the structure, the sample was dissolved in hot concentrated hydrochloric acid (37%) and subjected to ICP-OES analysis using five standards each for sodium and copper. The solution was found to contain 0.099 ± 0.070 ppm sodium and 28.8 ± 0.3 ppm copper, which confirmed negligible sodium content within the experimental uncertainty. The oxygen content of the material was confirmed with thermogravimetric analysis by placing 19.83 mg of the sample in an alumina pan and heating it to 500 °C at 1 °C/min under the reducing environment of 5% H_2/Ar mixture. The mass loss began at 380 °C and ended after 100 min. The sample was then cooled, and the mass loss was measured to be 2.60 mg corresponding to $\Delta m/m$ = 13.11%. Considering the formula Cu_2IrO_3, the expected $\Delta m/m$ = 13.07% was in excellent agreement with the observed value.

Crystal Structure. Figure 2 shows the PXRD pattern of Cu_2IrO_3 indexed in the space group $C2/c$, which is common among derivatives of the delafossite structure such as Na_2IrO_3, $CuNi_{2/3}Sb_{1/3}O_2$, and $CuCo_{2/3}Sb_{1/3}O_2$.[10,11] After an initial profile matching with the $C2/c$ space group, we naturally tried to draw atomic coordinates from the same model as the parent compound, Na_2IrO_3, where honeycomb layers of $(Ir_{2/3}Na_{1/3})O_6$ are stacked by NaO_6 octahedra (Figure 1). The Na_2IrO_3 model did not provide a good fit. We then took atomic positions from $CuNi_{2/3}Sb_{1/3}O_2$ where honeycomb layers of $(Ni_{2/3}Sb_{1/3})O_6$ are stacked by CuO_2 dumbbells[10] (Figure 1). The $CuNi_{2/3}Sb_{1/3}O_2$ model provided an excellent starting point for our refinement with the atomic positions listed in Tables 1 and 2. The c-axis in Cu_2IrO_3 is larger than in Na_2IrO_3 (11.51 Å versus 10.77 Å), but the monoclinic angles are nearly the same (99.03° versus 99.50°).[11] Therefore, Cu_2IrO_3 has larger interlayer spacing, $d = \frac{c}{2}\sin\beta$, with more 2D character.

The size broadening of the peaks was refined using spherical harmonics based on the $2/m$ Laue class. The region from 19 to 24° in Figure 2 shows asymmetric line broadening known as the Warren line shape,[17] which is common among the delafossite-type layered structures.[18] It is modeled as a number of small peaks merged together due to variations in the stacking of the honeycomb order from one plane to the next, known as stacking faults. An analysis of the Warren line shape yields about 10% stacking faults in the sample (Supporting Information). Similar patterns are observed in related layered materials including Na_2IrO_3,[11] $CuCo_{2/3}Sb_{1/3}O_2$,[10] and

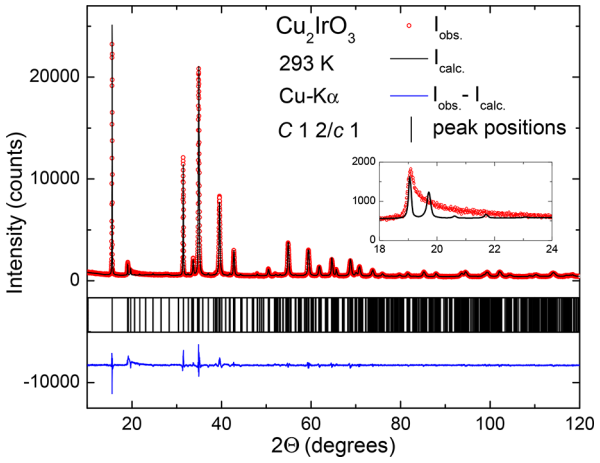

Figure 2. Room temperature powder X-ray diffraction pattern of Cu_2IrO_3. Experimental data are shown in red, Rietveld refinement in black, and the difference between observation and calculation in blue. Asymmetric broadening due to stacking faults in the range of 18−24° is magnified in the inset. Standard parameters for the Rietveld refinement and the Wyckoff positions are given in Tables 1 and 2.

Table 1. Crystallographic Data for Cu_2IrO_3 Obtained at Room Temperature Using Cu Kα Radiation with λ = 1.5406 Å[a]

unit cell parameters		refinement parameters	
space group	$C12/c1$	parameters	26
a (Å)	5.39331(5)	R_{Bragg} (%)	8.83
b (Å)	9.31118(9)	R_F (%)	10.5
c (Å)	11.51269(6)	R_P (%)	19.6
β (deg)	99.02916(1)	R_{wP} (%)	19.1
V (Å^3)	570.982(5)	R_{exp} (%)	8.06
Z	8	χ^2	5.6

[a]Unit cell dimensions and refinement parameters are reported. The region of stacking faults, between 18 and 24°, artificially increases the R factors (Figure 2). Excluding this region yields R_{wP} = 13.5, R_{exp} = 7.78, and χ^2 = 3.

Table 2. Wyckoff Sites, Atomic Coordinates, and Site Occupancies in the Crystal Structure of Cu_2IrO_3[a]

atom	site	x	y	z	occupancy
Ir1	8f	1/4	0.079(4)	0	0.81(1)
Cu1	8f	1/4	0.079(4)	0	0.18(9)
Ir2	4d	3/4	1/4	0	0.37(8)
Cu2	4d	3/4	1/4	0	0.62(2)
Cu3	4e	0	3/4	1/4	1
Cu4	4e	0	0.455(7)	1/4	1
Cu5	4e	0	0.080(5)	1/4	1
O1	8f	0.949(9)	3/4	0.090(8)	1
O2	8f	0.940(6)	0.420(7)	0.078(0)	1
O3	8f	0.932(6)	0.084(8)	0.091(6)	1

[a]The Debye−Waller (thermal) factors are reasonably low with B_{iso} = 1.0 Å^2 for copper and oxygen atoms and B_{iso} = 0.9 Å^2 for iridium atoms.

DOI: 10.1021/jacs.7b06911
J. Am. Chem. Soc. 2017, 139, 15371−15376

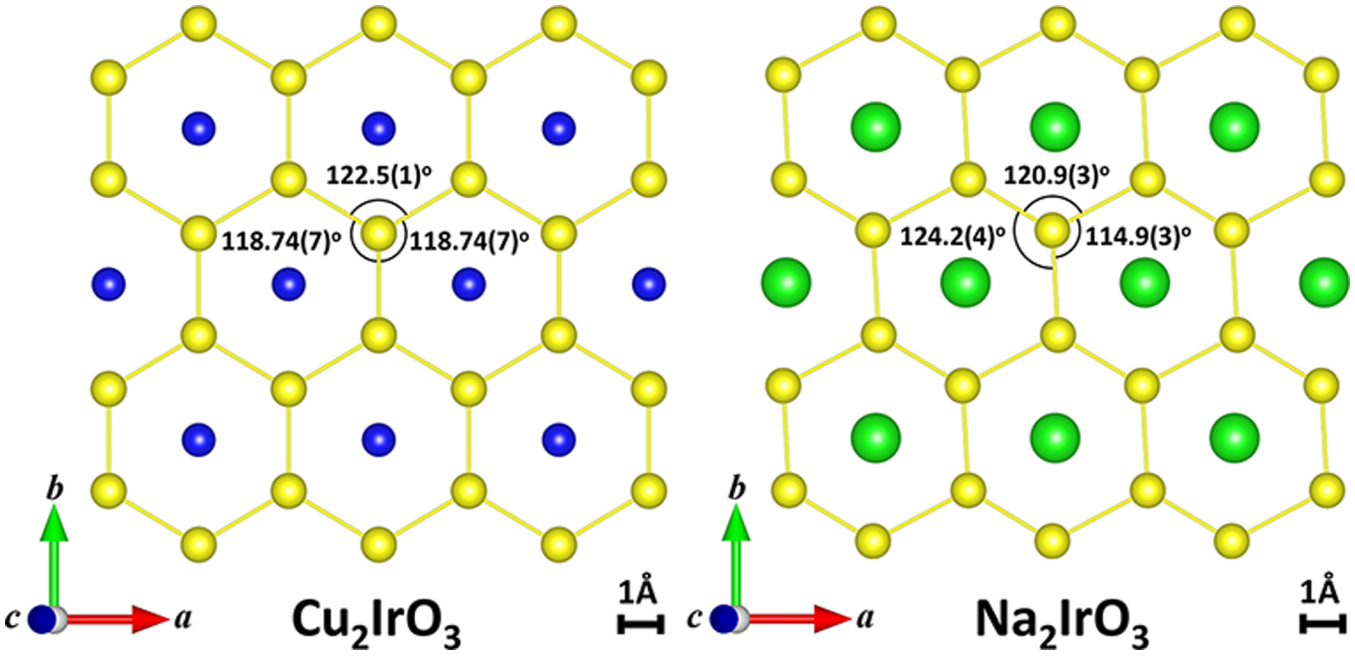

Figure 3. Planar view of the honeycomb ordering in Cu_2IrO_3 (left) and Na_2IrO_3 (right) to compare the Ir−Ir−Ir bond angles between the two materials in the same space group ($C2/c$). Yellow, blue, and green spheres represent Ir, Cu, and Na, respectively. Ir−Ir−Ir bond angles are closer to the ideal 120° in Cu_2IrO_3 compared to Na_2IrO_3 beyond the margin of error. The $C2/c$ structure of Na_2IrO_3 is taken from ref 11.

$NaCo_{2/3}Sb_{1/3}O_2$.[19] Figure 3 compares the honeycomb ordering, in the $a-b$ plane, between Na_2IrO_3 and Cu_2IrO_3. The Ir−Ir−Ir bond angles in Cu_2IrO_3 are closer to 120° than in Na_2IrO_3. The more 2D character and the more ideal bond angles bring Cu_2IrO_3 in closer proximity to the geometry of the Kitaev model.[5]

In a recent study,[20] similar mild conditions were applied to Na_2IrO_3 to exchange the interlayer sodium atoms but without exchanging the intralayer atoms:

$$Na_2IrO_3 + 1.5CuCl \rightarrow Cu_{1.5}Na_{0.5}IrO_3 + 1.5NaCl \quad (2)$$

The product has the same honeycomb layers as Na_2IrO_3, but the layers are stacked with copper dumbbells similar to the Cu_2IrO_3. The significance of the present work is to demonstrate that sodium can be exchanged with copper even inside the octahedral cages within the honeycomb layer.

Resistivity. Figure 4 shows the temperature dependence of resistivity in Cu_2IrO_3 from 50 to 300 K. The top left inset shows a poor fit to the Arrhenius expression $\rho \propto \exp(E_g/k_BT)$, where E_g is the energy gap. In a typical insulator, E_g is temperature-independent and much larger than k_BT, so $\log(\rho)$ scales linearly with T^{-1}. If the energy gap is temperature-dependent, a different behavior known as variable-range hopping (VRH) appears, where $\rho \propto \exp(E_g/k_BT^{1/(D+1)})$ in D dimensions.[21,22] The bottom right inset of Figure 4 shows a better fit to the 3D VRH expression, $\rho \propto \exp(E_g/k_BT^{1/4})$. A linear fit of $\log(\rho)$ to $T^{-1/4}$ indicates a "pseudogap" E_g = 825 meV in Cu_2IrO_3, the same order of magnitude as the optical gap measured in Na_2IrO_3 (340 meV).[23] Photoemission and spectroscopy experiments will be required for accurate evaluation of the optical gap in Cu_2IrO_3. A similar VRH behavior is observed in the parent compound Na_2IrO_3.[6] As previously explained for Sr_2IrO_4, Ir^{4+} has five electrons in the t_{2g} manifold with effective spin of 1/2. Strong spin−orbit coupling opens a gap in the t_{2g} manifold and drives the system toward a Mott insulator.[24] It is not clear why spin−orbit driven Mott

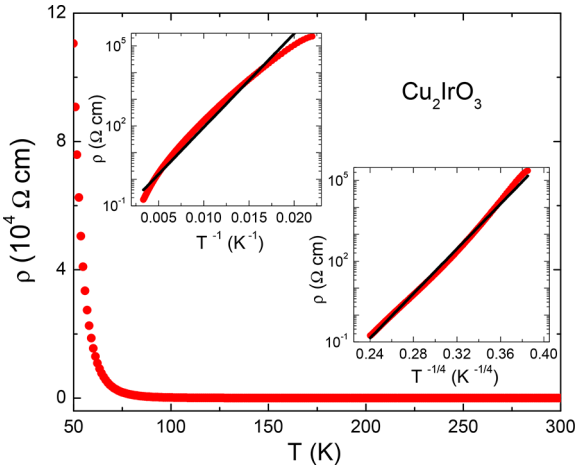

Figure 4. Resistivity plotted as a function of temperature in Cu_2IrO_3 showing insulator behavior. The top left inset shows that $\log(\rho)$ does not scale linearly with T^{-1}. The bottom right inset shows that $\log(\rho)$ scales better with $T^{-1/4}$.

insulators have a VRH instead of a conventional Arrhenius behavior.

Magnetization. Figure 5 shows the magnetic susceptibility (left y-axis) and the inverse susceptibility (right y-axis) as a function of temperature from 2 to 300 K in both Na_2IrO_3 and Cu_2IrO_3. The susceptibility data for both samples fit to the expression $\chi = \frac{C}{T-\Theta_{CW}}$ where the Curie−Weiss temperature Θ_{CW} is related to the magnetic exchange coupling and the Curie constant C is related to the effective magnetic moment, $\mu/\mu_B = \sqrt{3k_BC/N}$, with Avogadro number N and Boltzmann constant k_B. Our data on Na_2IrO_3 are consistent with previous reports.[5,6,25] The resulting magnetic moment $\mu_{eff} = 1.93(1)\mu_B$ in Cu_2IrO_3 is nearly identical to $1.89(1)\mu_B$ in Na_2IrO_3 and close to the expected moment 1.73 μ_B from Ir^{4+} with effective

DOI: 10.1021/jacs.7b06911
J. Am. Chem. Soc. 2017, 139, 15371−15376

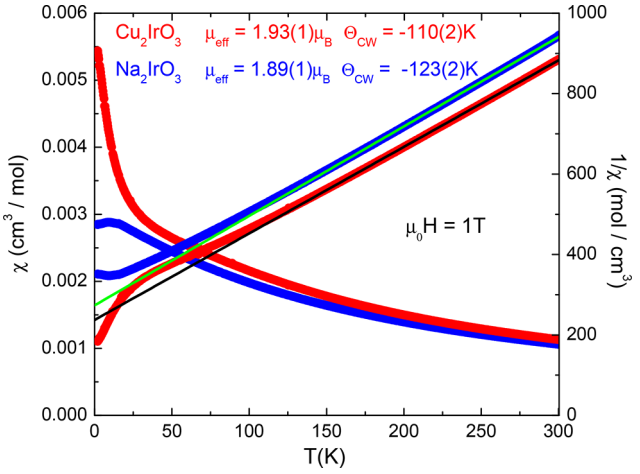

Figure 5. Molar magnetic susceptibility (left *y*-axis) and inverse susceptibility (right *y*-axis) as a function of temperature in Cu_2IrO_3 (red) and Na_2IrO_3 (blue). The effective magnetic moment and the Curie–Weiss temperature are reported on the figure from the Curie–Weiss fit in the range of 150–300 K. Fitting errors were evaluated by varying the fitting range.

$S = 1/2$. Figure 5 shows that $\chi(T)$ above 100 K is almost identical between Cu_2IrO_3 and Na_2IrO_3, with comparable Θ_{CW} and μ. However, below 100 K, the two curves differ. Na_2IrO_3 shows a clear peak at 15 K due to a long-range AFM order, but Cu_2IrO_3 maintains the Curie–Weiss behavior until 2.7 K.

Figure 6 shows that Cu_2IrO_3 orders at 2.7 K, much lower than $T_N = 15$ K in Na_2IrO_3. The ratio $f = |\Theta_{CW}|/T_N$, known as

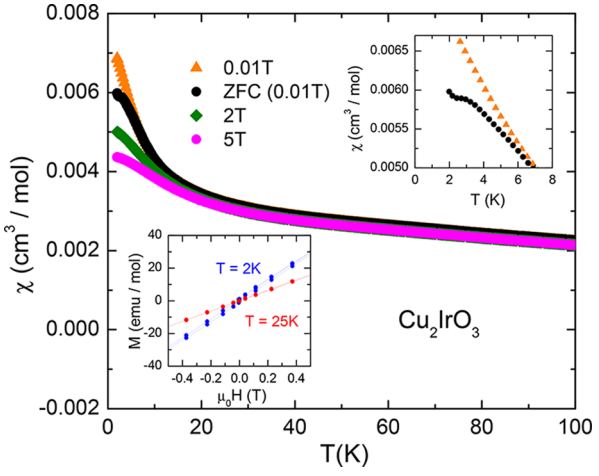

Figure 6. Molar susceptibility plotted as a function of temperature below 100 K to focus on the magnetic ordering. Top inset shows that Cu_2IrO_3 orders at 2.7 K with zero field cooling, but the order disappears in a weak magnetic field. The Curie tail below 10 K is suppressed by increasing field. Bottom inset shows a very small hysteresis at 2 K, which disappears at 25 K.

the frustration index,[1] is a rough measure of magnetic frustration. In Na_2IrO_3, the order of magnitude difference between $|\Theta_{CW}| = 123$ K and $T_N = 15$ K gives rise to $f = 8.2$. In Cu_2IrO_3, the frustration index increases significantly to $f = 40$, showing that the new copper iridate is even more frustrated than its parent compound and, therefore, is closer to a Kitaev spin liquid.[5,26] Two structural reasons could explain this: (a) the bond angles in the honeycomb layer of Cu_2IrO_3 are closer to the ideal 120° than in Na_2IrO_3 (Figure 3), and (b) the *c*-axis of Cu_2IrO_3 is larger than that of Na_2IrO_3 (Table 1). Figure 6 shows that the transition in Cu_2IrO_3 is weak; it is observable only by zero field cooling, disappears in the presence of a small field, and shows a small hysteresis. Such behavior could indicate a spin glass transition[27] with short-range (local) correlations instead of a long-range antiferromagnetic order.

Heat Capacity. Figure 7 compares the heat capacity in Cu_2IrO_3 with Na_2IrO_3.[6] The robust long-range AFM order is

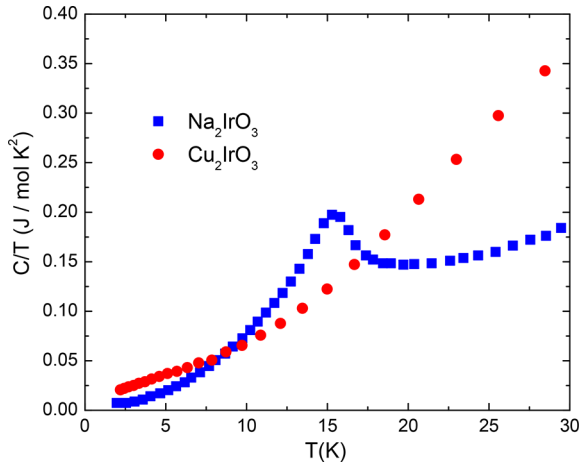

Figure 7. Heat capacity divided by temperature as a function of temperature in Cu_2IrO_3 (red circles) compared to Na_2IrO_3 (blue squares, from ref 6). Na_2IrO_3 shows a clear peak at the AFM transition $T_N = 15$ K. Such a peak is absent from the transition in Cu_2IrO_3 at 2.7 K.

marked by a peak at $T_N = 15$ K in the heat capacity of Na_2IrO_3. At this temperature, there is no evidence for magnetic ordering in Cu_2IrO_3. The heat capacity shows no sharp peak even at 2.7 K, where the weak order is observed in magnetic susceptibility. However, Cu_2IrO_3 exhibits a broad feature around 5 K, which could be evidence for short-range spin glass correlations.[27] In the Supporting Information, a T^3 lattice estimate is used to reveal a negligible entropy release (<5% $R\ln(2)$), near the transition, confirming the lack of long-range magnetic order. Curiously, in the limit of $T \rightarrow 0$, C/T approaches zero much slower in Cu_2IrO_3 than in Na_2IrO_3, which may be due to the proximity to the spin liquid phase. Our interpretation is that the FM Kitaev interaction in Cu_2IrO_3 is stronger than that in Na_2IrO_3 due to more favorable geometry of the honeycomb layers. In this scenario, the Kitaev interaction wins over the AFM Heisenberg interaction, which means Cu_2IrO_3 is closer to a Kitaev spin liquid than Na_2IrO_3. Further experiments such as NMR and neutron scattering are required to establish the true nature of magnetism in Cu_2IrO_3.

CONCLUSIONS

We demonstrate that it is possible to completely substitute all sodium atoms in Na_2IrO_3 with copper atoms through a topotactic reaction under mild conditions. The resulting material, Cu_2IrO_3, is the first copper iridium binary metal oxide and a new member of A_2IrO_3 honeycomb iridates. Structurally, Cu_2IrO_3 has honeycomb layers in a $C2/c$ unit cell similar to Na_2IrO_3, but the layers are linked by linearly coordinated CuO_2 dumbbells similar to $CuFeO_2$. Cu_2IrO_3 is an insulator with VRH behavior similar to Na_2IrO_3. From the Curie–Weiss analysis, iridium is in the 4+ oxidation state,

DOI: 10.1021/jacs.7b06911
J. Am. Chem. Soc. 2017, 139, 15371–15376

relevant to the Kitaev model and necessary for a spin liquid phase. Cu_2IrO_3 shows a weak magnetic order at 2.7 K with a frustration index of 40, which is an order of magnitude larger than Na_2IrO_3. The absence of a peak in the heat capacity data, the large frustration index, and the sensitivity of the magnetic transition to an external field are evidence for proximity to a quantum spin liquid. The structure of Cu_2IrO_3 provides a nearly perfect geometry for the Kitaev model with bond angles closer to the ideal 120° and a larger interlayer spacing compared to that of Na_2IrO_3.

■ ASSOCIATED CONTENT

Supporting Information

The Supporting Information is available free of charge on the ACS Publications website at DOI: 10.1021/jacs.7b06911.

Crystallographic data for Cu_2IrO_3 (CIF)
Additional details and figues as described in text (PDF)

■ AUTHOR INFORMATION

Corresponding Author

*fazel.tafti@bc.edu

ORCID

Fazel Tafti: 0000-0002-5723-4604

Notes

The authors declare no competing financial interest.

■ ACKNOWLEDGMENTS

F.T. is grateful to M. Graf, J. Carter, and J. O'Grady for their support during his lab construction. The work at Boston College was supported by BC starting budget and NSF Grant No. DMR-5104811. The work at Harvard and CNS was supported by the STC Center for Integrated Quantum Materials, NSF Grant No. DMR-1231319. This work was performed in part at the Center for Nanoscale Systems (CNS), a member of the National Nanotechnology Coordinated Infrastructure Network (NNCI), which is supported by the National Science Foundation under NSF Award No. 1541959. CNS is part of Harvard University.

■ REFERENCES

(1) Ramirez, A. P. *Annu. Rev. Mater. Sci.* **1994**, *24*, 453−480.
(2) Savary, L.; Balents, L. *Rep. Prog. Phys.* **2017**, *80*, 016502.
(3) Zhou, Y.; Kanoda, K.; Ng, T.-K. *Rev. Mod. Phys.* **2017**, *89*, 025003.
(4) Kitaev, A. *Ann. Phys.* **2006**, *321*, 2−111.
(5) Chaloupka, J.; Jackeli, G.; Khaliullin, G. *Phys. Rev. Lett.* **2010**, *105*, 027204.
(6) Singh, Y.; Gegenwart, P. *Phys. Rev. B: Condens. Matter Mater. Phys.* **2010**, *82*, 064412.
(7) Choi, S. K.; Coldea, R.; Kolmogorov, A. N.; Lancaster, T.; Mazin, I. I.; Blundell, S. J.; Radaelli, P. G.; Singh, Y.; Gegenwart, P.; Choi, K. R.; Cheong, S.-W.; Baker, P. J.; Stock, C.; Taylor, J. *Phys. Rev. Lett.* **2012**, *108*, 127204.
(8) Shannon, R. D.; Rogers, D. B.; Prewitt, C. T. *Inorg. Chem.* **1971**, *10*, 713−718.
(9) Effenberger, H. *Acta Crystallogr., Sect. C: Cryst. Struct. Commun.* **1991**, *47*, 2644−2646.
(10) Roudebush, J. H.; Andersen, N. H.; Ramlau, R.; Garlea, V. O.; Toft-Petersen, R.; Norby, P.; Schneider, R.; Hay, J. N.; Cava, R. J. *Inorg. Chem.* **2013**, *52*, 6083−6095.
(11) Krizan, J. W.; Roudebush, J. H.; Fox, G. M.; Cava, R. J. *Mater. Res. Bull.* **2014**, *52*, 162−166.
(12) Baroudi, K.; Yim, C.; Wu, H.; Huang, Q.; Roudebush, J. H.; Grafe, H.-J.; Kataev, V.; Buechner, B.; Ji, H.; Kuo, C.; Hu, Z.; Lee, J.; Mikhailova, D.; Hao Tjeng, L.; Cava, R. J. *J. Solid State Chem.* **2014**, *210*, 195−205.
(13) Cao, G.; Qi, T. F.; Li, L.; Terzic, J.; Cao, V. S.; Yuan, S. J.; Tovar, M.; Murthy, G.; Kaul, R. K. *Phys. Rev. B: Condens. Matter Mater. Phys.* **2013**, *88*, 220414.
(14) Manni, S.; Choi, S.; Mazin, I. I.; Coldea, R.; Altmeyer, M.; Jeschke, H. O.; Valenti, R.; Gegenwart, P. *Phys. Rev. B: Condens. Matter Mater. Phys.* **2014**, *89*, 245113.
(15) Rodríguez-Carvajal, J. *Phys. B* **1993**, *192*, 55−69.
(16) Salter, C. *J. Chem. Educ.* **2000**, *77*, 1239.
(17) Balzar, D. *J. Res. Natl. Inst. Stand. Technol.* **1993**, *98*, 321−353.
(18) Todorova, V.; Leineweber, A.; Kienle, L.; Duppel, V.; Jansen, M. *J. Solid State Chem.* **2011**, *184*, 1112−1119.
(19) Viciu, L.; Huang, Q.; Morosan, E.; Zandbergen, H. W.; Greenbaum, N. I.; McQueen, T.; Cava, R. J. *J. Solid State Chem.* **2007**, *180*, 1060−1067.
(20) Roudebush, J. H.; Ross, K. A.; Cava, R. J. *Dalton Trans.* **2016**, *45*, 8783−8789.
(21) Mott, N. F. *Philos. Mag.* **1969**, *19*, 835−852.
(22) Hill, R. M. *Phys. Status Solidi A* **1976**, *34*, 601−613.
(23) Comin, R.; Levy, G.; Ludbrook, B.; Zhu, Z.-H.; Veenstra, C. N.; Rosen, J. A.; Singh, Y.; Gegenwart, P.; Stricker, D.; Hancock, J. N.; van der Marel, D.; Elfimov, I. S.; Damascelli, A. *Phys. Rev. Lett.* **2012**, *109*, 266406.
(24) Kim, B. J.; Jin, H.; Moon, S. J.; Kim, J.-Y.; Park, B.-G.; Leem, C. S.; Yu, J.; Noh, T. W.; Kim, C.; Oh, S.-J.; Park, J.-H.; Durairaj, V.; Cao, G.; Rotenberg, E. *Phys. Rev. Lett.* **2008**, *101*, 076402.
(25) Mehlawat, K.; Thamizhavel, A.; Singh, Y. *Phys. Rev. B: Condens. Matter Mater. Phys.* **2017**, *95*, 144406.
(26) Nishimoto, S.; Katukuri, V. M.; Yushankhai, V.; Stoll, H.; Röbler, U. K.; Hozoi, L.; Rousochatzakis, I.; Brink, J. v. d. *Nat. Commun.* **2016**, *7*, 10273.
(27) Mydosh, J. A. *Spin Glasses: An Experimental Introduction*, 1st ed.; CRC Press: Boca Raton, FL, 1993.

DOI: 10.1021/jacs.7b06911
J. Am. Chem. Soc. 2017, 139, 15371−15376